Journal of Contaminant Hydrology 231 (2020) 103630

Contents lists available at ScienceDirect

Journal of Contaminant Hydrology

journal homepage: www.elsevier.com/locate/jconhyd

Humic acid induced weak attachment of fullerene nC_{60} nanoparticles and subsequent detachment upon reduction of solution ionic strength in saturated porous media

Zhan Wang[a,b], Tiantian Li[a], Chongyang Shen[a,*], Jianying Shang[a], Kaiyu Shi[a], Yulong Zhang[b], Baoguo Li[a,*]

[a] Department of Soil and Water Sciences, China Agricultural University, Beijing 100193, China.
[b] College of Land and Environment, Shenyang Agricultural University, Shenyang, Liaoning 110866, China.

ARTICLE INFO

Keywords:
nC_{60} nanoparticles
Colloid
Humic acid
Porous media
Transport

ABSTRACT

Sand column experiments were performed under saturated conditions to investigate impact of humic acid (HA) on attachment of nC_{60} nanoparticles (NPs) in NaCl and $CaCl_2$ at ionic strengths (ISs) from 1 mM to 100 mM and subsequent detachment via reducing solution IS. The attachment increased with increasing IS due to reduced repulsive Derjaguin-Landau-Verwey-Overbeek (DLVO) interaction energy and accordingly increased retention in primary energy wells. More attachments occurred in $CaCl_2$ compared to NaCl because Ca^{2+} exhibited greater charge screen ability and served as a bridging agent between the NPs and sand surfaces. The presence of HA significantly reduced nC_{60} NPs attachment on sand surfaces (especially on nanoscale physical heterogeneities) in 10 mM NaCl and 1 mM $CaCl_2$ because of enhanced electrostatic and steric repulsions. Interestingly, although the HA did not cause reduction of attachment in 100 mM NaCl and 10 mM $CaCl_2$ compared to the case in absence of HA, the HA caused weak attachment of nC_{60} on sand surfaces and then much more significant detachment by decreasing IS. The HA did not alter both attachment and detachment in 100 mM $CaCl_2$, because the Ca^{2+} at the high concentration caused formation of very stable complex of HA and NPs, and strong interaction of the complex with the sand surfaces via cation bridge. Our study highlighted that the HA can not only enhance the transport of NPs by inhibiting attachment as revealed in the literature, but also by the continuous capture and release of the NPs from surfaces in subsurface environments.

1. Introduction

Buckminsterfullerene (C_{60}), a hydrophobic molecule, consists of 60 carbon atoms with a spherical cage-like structure (Kroto et al., 1985; Li et al., 2008). The nC_{60} bears unique physicochemical characteristics such as antioxidation, and high electron affinity (Chen and Elimelech, 2006; Qu et al., 2012). Therefore, the C_{60} has gained a variety of applications including personal care products, pharmaceuticals, and new high-strength materials (Qu et al., 2012; Zhang et al., 2014a, 2014b; Haftka et al., 2015; McNew and LeBoeuf, 2016), The C_{60} can be synthesized in factories or generated in highly energetic nature events (e.g., lightning discharges) (Klaine et al., 2008; Zhang et al., 2012a, 2012b; Haftka et al., 2015; Sanchís et al., 2018). The production and use of C_{60} has caused its distribution in subsurface environments (Sanchís et al., 2012; Sanchís et al., 2015; Li et al., 2015).

Although the C_{60} has extremely low solubility in water, surface of the C_{60} can obtain negative charges in aqueous systems and stable nanoscale aggregates (nC_{60}) will be formed (Li et al., 2008). The resulting nC_{60} nanoparticles (NPs) persist in the environment because they are resistant to biodegradation (Kümmerer et al., 2011). However, the nC_{60} NPs were reported to be toxic to microbes (Chae et al., 2010), animals (Oberdorster, 2004), and human cells (Dhawan et al., 2006). In addition, the nC_{60} NPs can absorb a variety of inorganic and organic pollutants, and carry them to transport as a vehicle (i.e., the so-called colloid-facilitated transport of pollutants) (Li et al., 2002; Yang et al., 2006; Lin et al., 2010; Bai et al., 2013). Therefore, it is critical to understanding the mechanisms governing the nC_{60} NPs transport in the subsurface environments such as soil porous media for accurately evaluating their environmental risks.

Various studies (Chen and Elimelech, 2006, 2007, 2008; Li et al., 2008; Tong et al., 2010; Wang et al., 2010, 2012, 2016a; Chen et al., 2012) have examined the nC_{60} NPs deposition on collector surfaces and

* Corresponding authors.
E-mail addresses: chongyang.shen@cau.edu.cn (C. Shen), libg@cau.edu.cn (B. Li).

https://doi.org/10.1016/j.jconhyd.2020.103630
Received 30 October 2019; Received in revised form 4 January 2020; Accepted 20 February 2020
Available online 21 February 2020

their transport in porous media. These studies consistently showed that deposition of nC_{60} NPs can be qualitatively explained by the Derjaguin-Landau-Verwey-Overbeek (DLVO) theory. For example, increasing solution ionic strength (IS) reduces repulsive energy barrier. Hence, the nC_{60} NPs readily transport over the energy barrier at a higher IS and attach at primary energy minima (Wang et al., 2016a). The presence of nanoscale physical asperities (NPAs) and charge heterogeneities can locally reduce the interaction energy barrier and increase nC_{60} NPs deposition in primary minima (Li et al., 2008, 2017; Tong et al., 2010; Shen et al., 2018, 2019a, 2019b). However, the nC_{60} NPs deposited atop NPAs at primary minima can spontaneously detach even by Brownian diffusion because the NPAs can significantly reduce primary minimum depth and the adhesion acting on the NPs (Wang et al., 2016b). The secondary minima were shallow for the nC_{60} NPs, which may not cause the immobilization at the energy wells (Li et al., 2008).

The detachment of nC_{60} NPs in porous media has also been examined in the literature (Cheng et al., 2005; Wang et al., 2008; Hedayati et al., 2016). For example, Hedayati et al. (2016) examined transport of nC_{60} NPs in silica sand packed columns. They found that the nC_{60} NPs were detached by injection of deionized (DI) water and the amount of release of nC_{60} NPs was influenced by the IS at which the nC_{60} NPs were attached. Wang et al. (2008) showed that to fulfill substantial detachment of nC_{60} NPs retained in 100- to 140-mesh Ottawa sand required both decrease of solution IS and significant increase of pH. This indicated that the nC_{60} NPs were initially attached at deep primary minima. In addition to perturbation of solution chemistry, Cheng et al. (2005) illustrated that a sudden increase of flow rate could also cause the detachment of nC_{60} NPs.

As a major component of natural organic matter, humic acid (HA) is ubiquitous in soil and sediment environments (Li et al., 2018). Consequently, the HA and nC_{60} NPs likely encounter in the porous soil and sediments (Chae et al., 2012). It has been widely reported that the presence of HA reduced aggregation of nC_{60} NPs due to increase of electrostatic and steric repulsions between the NPs (Chen and Elimelech, 2007; Hyung et al., 2007; Duncan et al., 2008; Xie et al., 2008; Chae et al., 2012; Yang et al., 2013; Jung et al., 2014; Zhang et al., 2014a, 2014b; Li et al., 2018). Due to a similar reason, the HA enhanced the transport of nC_{60} NPs by reducing attachment on collector surfaces (Chen and Elimelech, 2008; Qu et al., 2012; Wang et al., 2012; McNew and LeBoeuf, 2016). However, the impact of HA on nC_{60} NPs aggregation and attachment was regulated by IS and cation valence (Franchi and O'Melia, 2003; Chen and Elimelech, 2008; Chae et al., 2012; Qu et al., 2012; McNew and LeBoeuf, 2016). While the aforementioned studies significantly improved knowledge of the mechanisms controlling the nC_{60} NPs attachment in porous media, very little attention has been paid to examining the influence of HA on detachment of nC_{60} NPs (i.e., the opposite mechanism of attachment). The coupled influence of HA and solution chemistry makes the nC_{60} NPs detachment even more complex and requires investigation.

This study, through carrying out saturated sand column experiments, systematically examined the impact of HA on nC_{60} NPs attachment in different electrolyte solutions (NaCl and $CaCl_2$) with different ISs and subsequent detachment by IS reduction. We found that while the HA reduced deposition of nC_{60} NPs, it also caused a fraction of nC_{60} NPs weakly attached on sand surfaces and then released upon solution IS reduction. The detachment of nC_{60} NPs by the HA was more significant if the NPs were initially deposited in NaCl at higher ISs, but was completely inhibited in $CaCl_2$ at high ISs. The findings in this study have important implication to water and wastewater filtration using membranes and developing mathematical models for predicting mobility of NPs in subsurface environments.

2. Materials and methods

2.1. Quartz sand

Quartz sand with sizes between 210 μm and 297 μm was used as collectors to pack the columns, which was obtained from Sigma-Aldrich (St. Louis, Missouri, United States). The approach of Zhuang et al. (2005) was used to clean the sand grains. Surface morphologies of the cleaned sand were measured via a Hitachi S4300 scanning electron microscope (SEM) (Hitachi Corp., Tokyo, Japan). The fine fraction of the sand was isolated via sonication and used to determine zeta potentials in NaCl and $CaCl_2$ at different solution ISs via a ZetaPlus (Brookhaven Instruments Corp., Holtesville, New York) (Zhou et al., 2011; Wang et al., 2016a).

2.2. Fullerene NPs suspension

Fullerene C_{60} powder (99.9% purity) produced by Sigma-Aldrich (St. Louis, Missouri, United States) was used. The method used to prepare the nC_{60} NPs stock suspension can be found in our previous study (Wang et al., 2016a). Briefly, the total organic carbon (TOC) of the prepared nC_{60} NPs stock suspension was determined to be 9 mg L^{-1} using a TOC analyzer (TOC-V_{CPN}, Shimadzu, Japan). The nC_{60} NPs influent suspensions for column experiments were prepared by adding the nC_{60} stock suspension into NaCl or $CaCl_2$ electrolyte solution at different ISs. The resulting ISs of the influent suspensions were 1 mM, 10 mM, or 100 mM, with the concentration of nC_{60} to be 1.8 mg L^{-1} by diluting the stock solution. The dynamic light scattering (Zetasizer Nano ZS, Malvern Instruments Ltd., Southborough, Massachusetts, United States) was used to measure the sizes and zeta potentials of the nC_{60} NPs in the influent suspensions at different chemical conditions. The zeta potentials of the nC_{60} NPs were determined using a ZetaPlus analyzer (Brookhaven Instruments Corp., Holtesville, New York, United States).

2.3. Humic acid suspension

Similar to Chen and Elimelech (2007), the humic acid suspension was obtained by adding 50 mg of humic acid powder (Sigma-Aldrich, St. Louis, Missouri, United States) in 100 mL DI water. The suspension was stirred for 24 h under dark conditions, and passed through a 0.22 μm filter membrane. Using the TOC analyzer (TOC-V_{CPN}, Shimadzu, Japan), TOC content of the humic acid suspension was determined to be ~210 mg L^{-1}. The HA was added into some nC_{60} NPs suspensions to result in a concentration of 5 mg L^{-1} of the HA for zeta potential measurements and column transport experiments.

2.4. Column transport experiments

Acrylic columns (3-cm inner diameter and 10-cm long) were adopted to implement the column experiments. The method of Wang et al. (2016a) was used to pack the columns. Briefly, a wet-packing method was used to ensure saturation of the column systems. The sand was slowly added into the columns filled with water with gentle vibrations to avoid layering and air entrapment. The porosities of the columns were calculated to be 0.36 by using the mass of the sand and assuming sand density of 2.65 g cm^{-3}.

A Darcy velocity of 4.32 m d^{-1} was employed for all column transport experiments. To standardize the physicochemical conditions of the column systems, background NaCl or $CaCl_2$ electrolyte solution at pH 7 (adjusted using 0.1 mM $NaHCO_3$) was first injected into the columns upward for over 20 pore volumes (PVs). Then the column was flushed with 10 PVs of nC_{60} NPs influent suspension with or without HA (1.8 mg L^{-1} of nC_{60} and 5 mg L^{-1} of HA) at pH 7 (denoted as Phase 1), 5 PVs of NP-free electrolyte solution (Phase 2), and finally DI water (Phase 3). This three-step procedure has been widely employed in

previous studies (Shen et al., 2012; Wang et al., 2016b; Li et al., 2017) to examine colloid attachment and detachment in porous media. Effluent suspensions of the column experiments were collected by an automatic collector (BSZ-100, Huxi Instrument Corp., Shanghai, China), and the concentration of nC_{60} NPs was measured by a UV–vis spectrophotometry (DU Series 800, Beckman Instruments, Inc., Fullerton, California, United States) at a wavelength of 550 nm. The effluents at high ISs were sonicated to ensure the monodispersion before the measurements.

2.5. Calculation of DLVO interaction energies

To reveal the mechanisms controlling nC_{60} NPs attachment and detachment, it is necessary to determine the DLVO interaction energies between the NPs and the sand surfaces (Ryam and Elimelech, 1996; Ninham, 1999; Hoek and Agarwal, 2006; Wang et al., 2008). The surface element integration (SEI) technique, developed by Bhattacharjee and Elimelech (1997), was employed for performance of the interaction energy calculations. Note that the Derjaguin (DA) approach has been traditionally used to calculate the interaction energies. This approach, however, contains several assumptions in the calculations, as have been summarized in Shen et al. (2019a). Specifically, the DA approach did not consider the curvature effect of particle surface and assumed that the interaction energy for a particle is only due to a small region of the particle surface that is closet to the interacting surface. The SEI technique has overcome the limitations existing in the DA approach and can give accurate calculations of interaction energy for colloids even at nanoscale (Lin and Wiesner, 2012).

The total DLVO energy was taken as a sum of van der Waals (VDW) attractive interaction energy, electrical double layer (DL) interaction energy, and short-range repulsion. The short-range repulsion was included by determining Born (BR) repulsion, as adopted in previous studies (Hoek and Agarwal, 2006; Bradford and Torkzaban, 2013; Seetha et al., 2015; Shen et al., 2018). The nC_{60} NPs were assumed to be spherical and the sand surface was taken as plate. The use of SEI technique to calculate energies for sphere-plate interaction can be referred to previous studies (Wang et al., 2016a, 2016b; Li et al., 2017; Shen et al., 2018). Briefly, surfaces of both a NP and sand were discretized into small area elements. The VDW, DL, and BR differential interaction energies between each pair of area elements on the NP and sand surfaces were determined using the expressions developed by Hamaker (1937), Hogg et al. (1966), and Oliveira (1997), respectively. Summing of the VDW, DL, and BR differential interaction energies for all pairs of area elements resulted in the total interaction energy for a nC_{60} NP.

Considerable wedge-like depressions existed in the sand surfaces, as will be shown later in the paper. To reveal the role of the wedge-like depressions in nC_{60} NPs attachment, the depressions were represented by two intersecting half planes and the interaction force between a nC_{60} NP and the model concave surface was determined (Fig. 1). Li et al. (2017) has shown detailed procedure for calculating interaction force for the aforementioned interaction configuration. Briefly, the Cartesian coordinate system was used for the interaction configuration in Fig. 1. The *z* axis passed through the line where the two half planar surfaces intersect, and the two intersecting half planar surfaces were bisected by the *y*-*z* plane. The total forces along the *x*- (F_x) and *y*-direction (F_y) were equal to $F_1\cos\left(\frac{\alpha}{2}\right) - F_2\cos\left(\frac{\alpha}{2}\right)$.and $F_1\sin\left(\frac{\alpha}{2}\right) + F_2\sin\left(\frac{\alpha}{2}\right)$, respectively, where α is the angle between the two half planes, and F_1 and F_2 are the interaction forces between the nC_{60} NP and the left and right half planar surface, respectively. The values of F_1 or F_2 were determined using the SEI technique. The calculation procedure was the same as that for determining interaction energy shown in the previous section. However, differential VDW, DL, and BL forces between area elements were determined (Li et al., 2017) instead of calculating differential interaction energies.

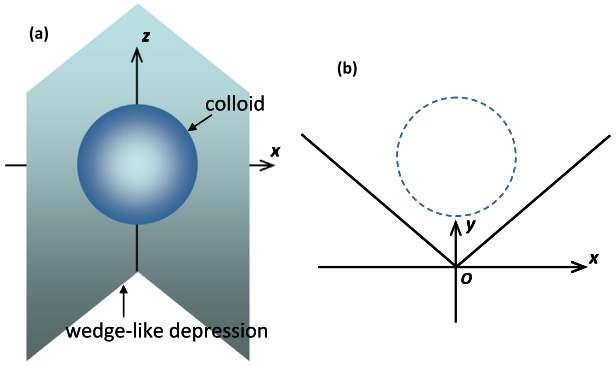

Fig. 1. Schematic illustration of interaction between a spherical colloid and a wedge-like depression consisting of two half planes. (b) is plan view image of the interaction configuration of (a). Modified from Shen et al. (2018).

As will be showing in the following, the nC_{60} NPs were aggregated at high ISs. However, we still used the sizes of the primary particles of the nC_{60} aggregates for interaction energy calculations at the high ISs. This is because the colloidal interaction energy for aggregated particles was similar to those of the primary particles, but was much smaller than that for an equivalent sphere (e.g., a sphere with the same volume as that of the aggregate) (Lin and Wiesner, 2012).

3. Results and discussion

3.1. Characteristics of nC_{60} NPs and collectors

The nC_{60} NPs used had the same properties as those used in our previous study (Wang et al., 2016a), which were spherical in shape with slight angular features accord to transmission electron microscope (TEM) examinations. Table 1 shows measured zeta potentials of nC_{60} NPs and collector grains, and sizes of the NPs in electrolyte solutions at different ISs with or without HA. The zeta potentials were negative for both the NPs and sand grains under all chemical conditions except at 100 mM $CaCl_2$. The existence of positive zeta potentials in $CaCl_2$ at the high IS was due to sorption of Ca^{2+} on the NP and sand surfaces, causing charge reversal (Kuznar and Elimelech, 2004). The presence of HA caused more negative zeta potentials of the NPs and sand grains, which is in agreement with the results in previous studies (Dhawan et al., 2006; Chen and Elimelech, 2007; Zhang et al., 2014a, 2014b; Lin et al., 2017). This is because adsorption of the HA onto the nC_{60} NPs and sand surfaces increased the negative charges and accordingly resulted in more negative zeta potentials (Zhang et al., 2009; Qu et al., 2012; Wang et al., 2012). Previous studies (Xie et al., 2008; Qu et al.,

Table 1
Sizes of nC_{60} NPs and zeta potentials of the nC_{60} NPs and sand under different chemical conditions.

Electrolyte	IS (mM)	Sizes of the NPs (nm)	Zeta potential (mV)	
			nC_{60} NPs	Sand
DI water	0.1	125 ± 0.9	−31.6 ± 0.55	−58.2 ± 6.3
NaCl	1 (HA)	119 ± 0.2	−27.4 ± 3.7	−51.6 ± 8.6
	1	122 ± 0.6	−24.5 ± 3.6	−49.3 ± 9.4
NaCl	10 (HA)	119 ± 0.2	−18.1 ± 0.43	−35.9 ± 3.7
	10	133 ± 2.0	−14.6 ± 4.4	−32.5 ± 2.8
NaCl	100 (HA)	119 ± 0.3	−9.0 ± 0.64	−23.2 ± 2.8
	100	239 ± 22.2	−8.3 ± 0.6	−20.7 ± 4.0
$CaCl_2$	1(HA)	119 ± 0.9	−20.5 ± 3.5	−33.5 ± 3.3
	1	132 ± 1.4	−16.8 ± 2.56	−30.0 ± 5.2
$CaCl_2$	10 (HA)	416 ± 18.5	−15.6 ± 3.1	−13.7 ± 0.5
	10	422 ± 25.5	−8.3 ± 2.63	−11.6 ± 2.5
$CaCl_2$	100 (HA)	653 ± 25.8	7.2 ± 0.4	1.5 ± 0.3
	100	686 ± 29.3	5.9 ± 0.54	3.9 ± 1.3

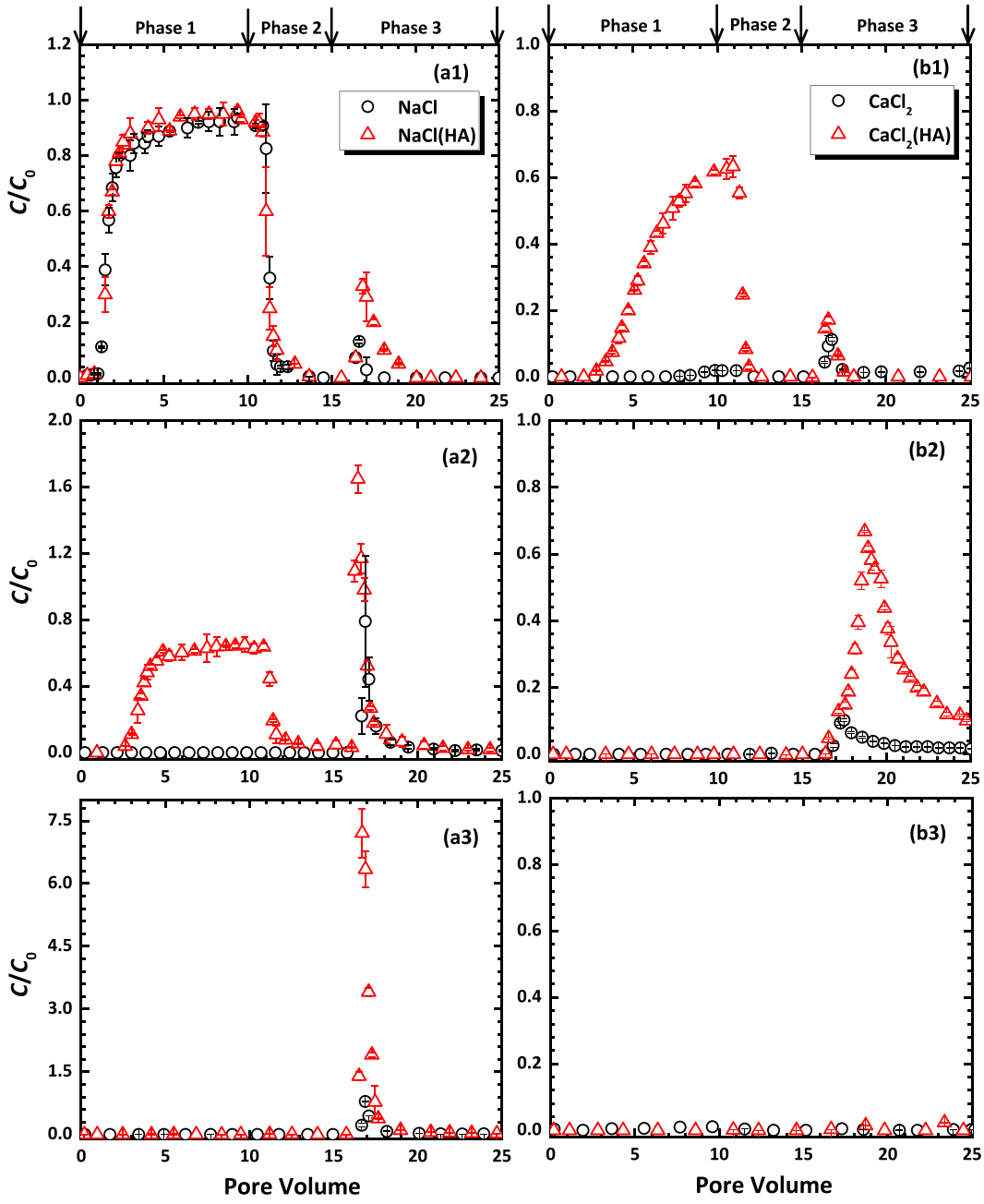

Fig. 2. BTCs for transport of nC_{60} NPs in (a) NaCl and (b) $CaCl_2$ solutions with (red symbols) or (black symbols) without HA at different ISs (1, 1 mM; 2, 10 mM; 3, 100 mM). (For interpretation of the references to colour in this figure legend, the reader is referred to the web version of this article.)

2012) showed that the HA increased stability of nC_{60} NPs suspensions and reduced the sizes of nC_{60} NPs aggregates by increasing electrostatic and steric repulsions. Indeed, the results in Table 1 showed that the sizes of the nC_{60} NPs were similar at all ISs in NaCl if the HA was present due to inhibition of aggregation, while the size of the nC_{60} NPs increased with increasing IS in NaCl without HA. However, the size of the nC_{60} NPs still increased with increasing IS in $CaCl_2$ even if the HA was present. This is likely due to the formation of the complexes of HA and NPs via cation bridge (Chen and Elimelech, 2007). As will be shown later by SEM examinations in the paper, reticular complexes on the sand surfaces were formed in $CaCl_2$.

3.2. Attachment of nC_{60} NPs

Fig. 2 presents breakthrough curves (BTCs) for the nC_{60} NPs by plotting the value of C/C_0 as a function of PV, where C and C_0 are effluent and influent NP concentrations, respectively. In phase 1, the nC_{60} NPs were attached on sand surfaces in NaCl or $CaCl_2$ at different ISs. Higher IS caused more attachments of nC_{60} NPs, as have been observed in previous studies (Chen and Elimelech, 2006, 2007, 2008; Li et al., 2008; Chae et al., 2012; Qu et al., 2012; Bai et al., 2013; McNew and LeBoeuf, 2015, 2016). The results confirmed that the nC_{60} can acquire negative surface charge (although the mechanism is still unclear to date), and the attachment of the nC_{60} was controlled by the electrostatic interaction in the electrolytes (Chen and Elimelech, 2006). The increase of attachment with IS can be qualitatively explained by the energy calculations in Fig. 3 and Table 2. Specifically, increasing IS reduces repulsive energy barrier and thereby increases attachment in primary energy wells. At a given IS, the nC_{60} NPs attachment was more in $CaCl_2$ than in NaCl. This is because the Ca^{2+} was more effective for screening the DL repulsion and can link the NPs to the sand surfaces (i.e., the cation bridge effect) (Schijven and Hassanizadeh, 2000).

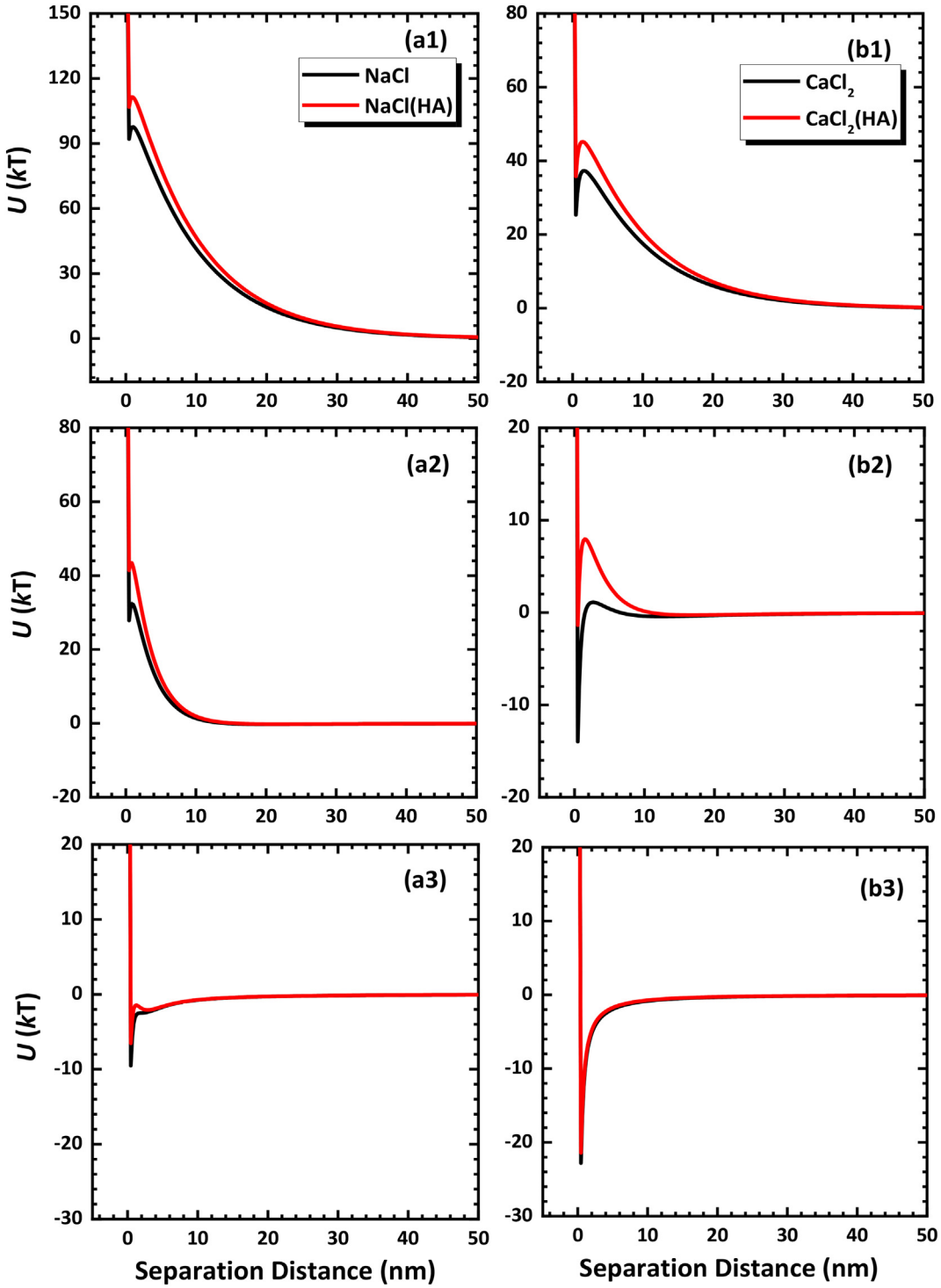

Fig. 3. Calculated DLVO interaction energies between a nC_{60} NP and a sand surface in (a) NaCl and (b) $CaCl_2$ solutions at different ISs (1, 1 mM; 2, 10 mM; 3, 100 mM) with (red) or without HA (black) copresent. (For interpretation of the references to colour in this figure legend, the reader is referred to the web version of this article.)

It should be noted that the attachment of nC_{60} NPs in the sand cannot be quantitatively explained by the interaction energy calculations. For instance, the calculations showed that the interaction energy barriers were much greater than the average kinetic energy of a colloid (1.5 *k*T, *k* is Boltzmann constant, T is absolute temperature) in NaCl at IS ≤ 10 mM and in $CaCl_2$ at 1 mM. These large repulsive energy barriers essentially inhibit the approach of nC_{60} NPs to primary wells of interaction energy profiles. Thus, attach at primary energy minima cannot occur under these chemical conditions. The prediction by the calculations, however, was in contrast to the aforementioned experimental observations. The SEM images (Fig. 4) showed that the sand surfaces were very rough, which contained considerable NPAs. The NPAs can increase primary minimum attachment by locally reducing repulsive energy barrier under unfavorable conditions (Shen et al., 2012a, 2012b; Zou et al., 2015; Rasmuson et al., 2017). In addition, the sand surfaces may bear charges different from those of bulk sand surfaces (Shen et al., 2015; Li et al., 2017). The primary minimum attachment can be further enhanced if the NPAs bear charges different

Table 2
The values of primary minimum depths (U_{pri}), maximum energy barriers (U_{max}), and secondary minimum depths (U_{sec}) and distances for the DLVO interaction energy profiles in Fig. 3. N.A., absence of energy minimum.

Electrolyte	IS (mM)	U_{pri} (kT)	U_{max} (kT)	U_{sec} (kT)	
				Depth (kT)	Distance (nm)
NaCl	1(HA)	4.6	111.4	0.012	101.46
	1	5.7	97.7	0.012	104.86
NaCl	10(HA)	2.0	43.4	0.19	21.86
	10	4.5	32.4	0.25	20.46
NaCl	100(HA)	4.5	N.A.	N.A.	N.A.
	100	5.6	N.A.	N.A.	N.A.
$CaCl_2$	1(HA)	9.43	45.2	0.015	90.66
	1	12.0	37.3	0.020	85.66
$CaCl_2$	10(HA)	9.3	7.95	0.32	16.66
	10	15.1	1.12	0.43	12.46
$CaCl_2$	100(HA)	21.4	N.A.	N.A.	N.A.
	100	22.8	N.A.	N.A.	N.A.

Note: N.A., absence of energy minimum.

from those of bulk collector surfaces (i.e., physical and chemical heterogeneities are coupled). The reason is that the existence of chemical heterogeneity can increase the depth of primary minimum, which could compensate for the reduction effect of NPAs on primary minimum depth (Bradford and Torkzaban, 2013; Shen et al., 2018, 2019a). Colloids cannot be immobilized if the primary energy wells are very shallow due to existence of Brownian diffusion.

In addition to the NPAs, Fig. 4 shows that the sand surfaces also contained large wedge-like depressions. To interpret the role of the wedge-like depression in nC_{60} NPs attachment and detachment, the interaction forces between a nC_{60} NP and the depression were calculated using the method in Materials and Methods. Fig. 5 shows the maps of F_x and F_y for a nC_{60} NP interacting with the depression on the x-y plane in 1, 10, and 100 mM NaCl. The force maps were generated by changing the (x, y) positions of the NP in a rasterized manner. In the dark areas, the forces were ignored because they could not be determined due to physical overlap between the nC_{60} NP and the surface. The scale bar to the top of each plot indicates the forces in units of $\times 10^{-12}$ N. Fig. 5 shows that when the NP is close to the tip of the concave surface, the repulsive energy barrier could be eliminated even at low ISs (e.g., 1 mM). This is because the repulsion between the NP and a half surface was eliminated by the repulsion from the other half surface in the opposite direction. Therefore, the nC_{60} NPs were favored to be attached in primary minima at the locations of concave surfaces where the repulsive energy barrier was eliminated.

In addition to surface physical and heterogeneities, aggregation of nC_{60} NPs (see Fig. 4) may also increase retention of the nC_{60} NPs (Taghavy et al., 2015; Babakhani, 2019). While the aggregation of colloids does not significantly alter the interaction energies (Lin and Wiesner, 2012), it could increase retention via enhanced sedimentation

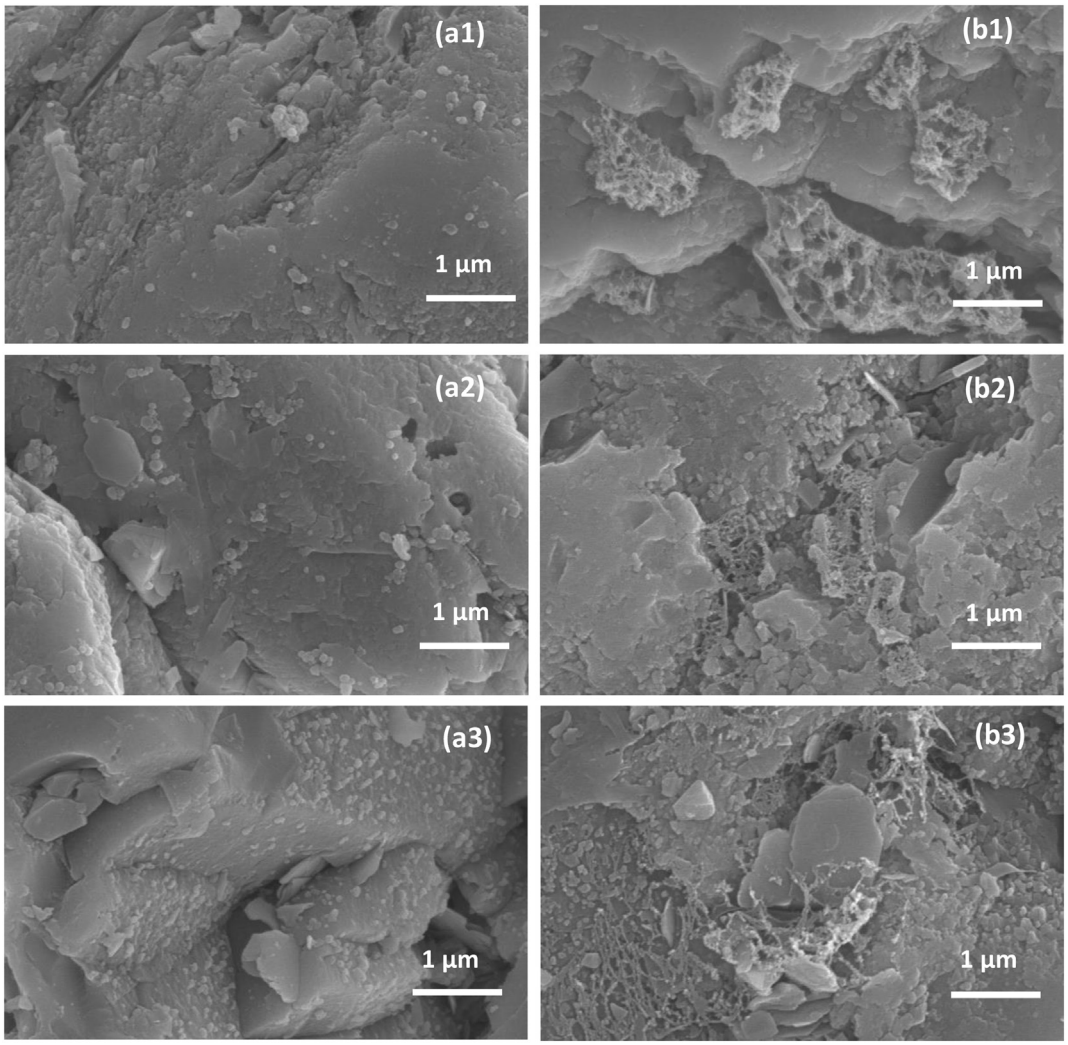

Fig. 4. SEM images of sand surface with attachment of nC_{60} NP in $CaCl_2$ at different ISs (1, 1 mM; 2, 10 mM; 3, 100 mM) (a) without or (b) with the presence of HA.

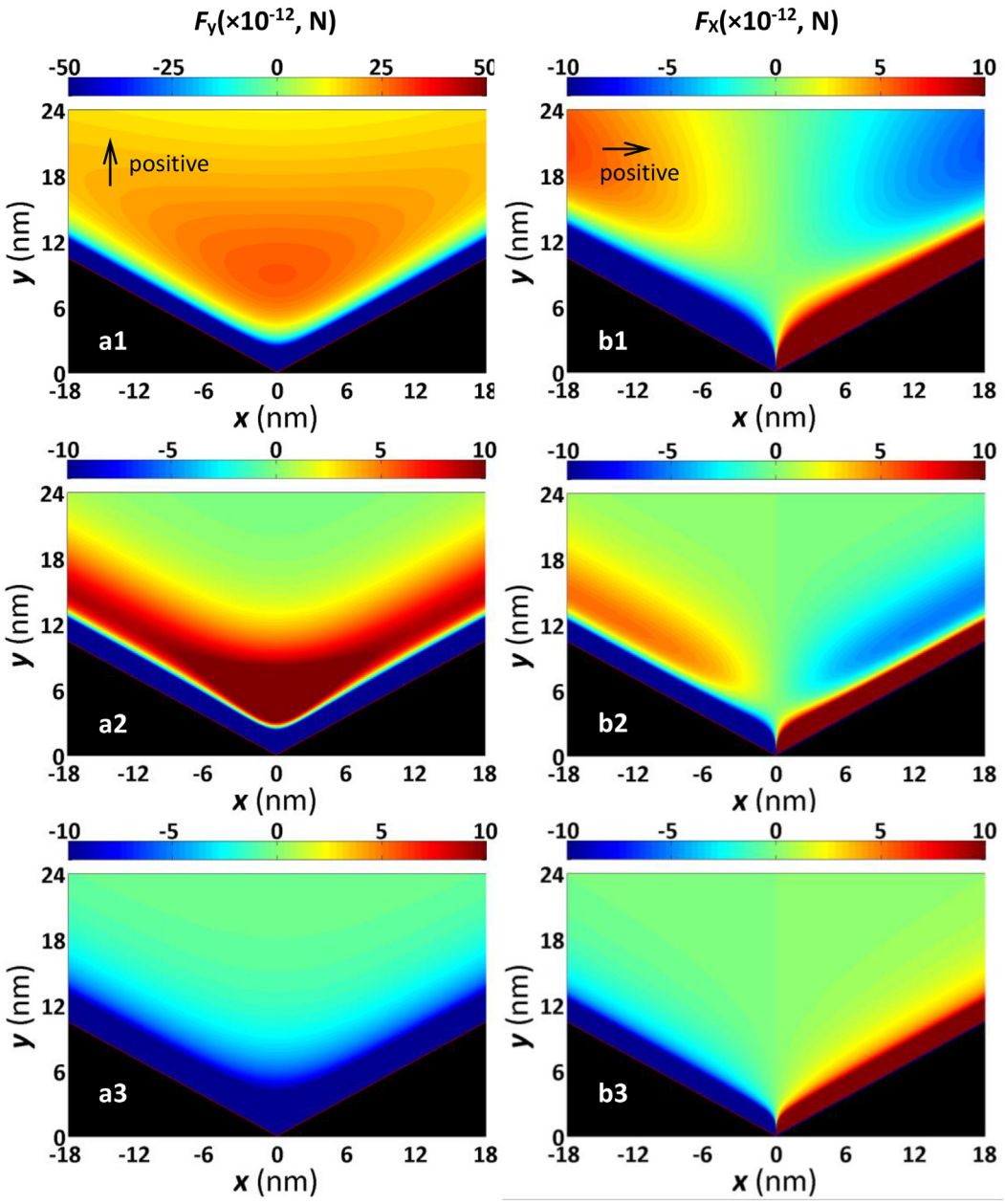

Fig. 5. Maps of DLVO interaction force components in (a) *y*- and (b) *x*-directions for a nC_{60} NP interacting with the two intersecting half planes on the *x*-*y* plane at $z = 0$ at 1 mM, 10 mM, and 100 mM NaCl. The angle of the two intersecting half planes was 120 degree. In the black regions, the interaction force was not calculated becasue of physical overlap between the NP and the concave surface. The scale bar to the top of each plot indicates the interaction force in units of $\times 10^{-12}$ N. In (a) and (b), positive values represent the force components along positive *y*-direction and *x*-direction, respectively.

and straining (Porubcan and Xu, 2011; Chrysikopoulos and Syngouna, 2014). Notably, the calculated secondary minima depths were much smaller than the average kinetic energy of a colloid. Hence, the secondary minima should not play a significant role in nC_{60} NPs attachment. Similarly, Li et al. (2008) showed that the secondary minimum depths were extremely small for the nC_{60} NPs, which had minor influence on the deposition of nC_{60} NPs in sand porous media.

Fig. 2 shows that HA reduced the deposition of nC_{60} NPs attachment in the sand. As shown in Table 1, the zeta potentials of both nC_{60} NPs and sand surface were increased when the HA was present. Accordingly, the DL repulsion and interaction energy barrier were increased by the presence of HA (see Fig. 3 and Table 2), causing reduction of the attachment in primary minima. In addition, the presence of HA increases steric repulsion (Chen and Elimelech, 2008; Zhang et al., 2013; Yang et al., 2019), which can reduce or even eliminate primary energy well (Table 2) and thus decrease attachment in primary minima (Wang et al., 2016b). It should be mentioned that the reduced attachment by the HA was only significant in 10 mM NaCl and 1 mM $CaCl_2$. There was only a minor reduction of attachment of the NPs by the HA in 1 mM NaCl. No influence of attachment by the HA existed in NaCl at 100 mM and in $CaCl_2$ at 10 mM and 100 mM (i.e., complete attachment both in the presence and absence of HA).

Two reasons may explain above minor influence of HA on nC_{60} NPs attachment at 1 mM NaCl. First, the HA had low sorption on surfaces of the nC_{60} NPs and sand in NaCl at this low IS (Qu et al., 2012). Second, the nC_{60} NPs were attached in sites where deep primary minima existed at this IS. The NPs could still attach at these energy wells even if these primary minima were decreased to a certain degree due to the electrostatic and steric repulsion by the HA. One possible attachment site is large charge heterogeneity which can significantly reduce or even

Table 3
Fractions of nC_{60} NPs recovered from phase 1 and phase 2 (M_{12}), phase 3 (M_3), total recovered particles ($M_T = M_{12} + M_3$), and irreversibly attached colloids ($M_I = 1\text{-}M_T$) for BTCs of column transport experiments in Fig. 2.

Electrolyte	IS (mM)	M_{12}		M_3		$M_3/(1 - M_{12})$		M_T		M_I		$M_I/(1 - M_{12})$	
		HA	N.A.	HA	N.A.	HA	N.A.	HA	N.A.	HA	N.A.	HA	N.A.
NaCl	1	0.88	0.86	0.06	0.005	0.49	0.04	0.94	0.86	0.06	0.14	0.51	0.96
NaCl	10	0.40	0	0.15	0.10	0.24	0.1	0.54	0.1	0.46	0.9	0.76	0.9
NaCl	100	0.002	0	0.45	0.06	0.46	0.06	0.46	0.06	0.54	0.94	0.55	0.94
$CaCl_2$	1	0.36	0.005	0.013	0.02	0.02	0.02	0.38	0.02	0.63	0.98	0.98	0.98
$CaCl_2$	10	0	0	0.22	0.007	0.22	0.007	0.22	0.01	0.78	0.99	0.78	0.99
$CaCl_2$	100	0.001	0	0.006	0	0.006	0	0.006	0	0.99	1	0.99	1

Note: N.A., absence of HA in the electrolyte.

eliminate the large energy barrier that exist at low solution ISs and cause very deep primary energy wells (Shen et al., 2013). In addition, Fig. 5 shows that the interaction energy barrier and primary minimum depth can also be decreased and increased at concave surfaces, respectively. Li et al. (2017) conducted column experiments and SEM examinations, showing that colloids were preferentially attached in primary minima at large charge heterogeneities and/or concave surfaces at low solution ISs. The primary minimum was very shallow or even absent in the interaction energy profiles atop the NPAs without charge heterogeneities copresent at low ISs (Shen et al., 2012a, 2019a; Bradford and Torkzaban, 2013). Therefore, the nC_{60} NPs attachment on NPAs may not be significant at 1 mM NaCl. In 10 mM NaCl and 1 mM $CaCl_2$ solutions, the NPAs may become available for attachment of nC_{60} NPs if the primary minima were increased to be deep enough to immobilize NPs. However, the attachment at the NPAs was readily influenced by the HA. Specifically, the NPAs may be again unfavorable for attachment if the primary minimum were decreased by the HA (Wang et al., 2016a, 2016b). This could explain why the HA caused significant transport of nC_{60} NPs at 10 mM NaCl and 1 mM $CaCl_2$, whereas nearly complete deposition occurred when the HA was absent. In NaCl at 100 mM and in $CaCl_2$ at 10 mM and 100 mM, the primary minima were further increased atop NPAs, which could immobilize the NPs even in the presence of HA. Therefore, complete attachment occurred under these chemical conditions both in the presence and absence of HA.

3.3. Detachment of nC_{60} NPs

In phase 2 of Fig. 2, the nC_{60} NPs that were unattached in pore water were displaced out of the columns by injection of NP-free electrolyte solution. Small tails existed in the BTCs in 1 mM and 10 mM NaCl with HA present, which were probably due to spontaneous release of the nC_{60} NPs from primary minima through Brownian diffusion. The spontaneous release from primary minimum could occur when the decreased primary minimum depths by both NPAs and HA were comparable to the average kinetic energy of a colloid (Wang et al., 2016a, 2016b). Note that if there were nC_{60} NPs attached at shallow secondary energy wells, they could also spontaneously detach by Brownian diffusion and cause the BTC tails (Li et al., 2005; Shen et al., 2016a, 2016b).

In phase 3 of BTCs in Fig. 2, the flush of DI water caused a fraction of attached nC_{60} NPs released, as denoted by the peaks in the BTCs. It has been traditionally regarded that only colloids that were attached at secondary energy wells could be detached by IS reduction because the secondary minimum depth decreases with decreasing IS (Hahn and O'Melia, 2004; Hahn et al., 2004). Colloid attachment in primary minimum is irreversible because the primary energy wells are deep at all solution ISs. These viewpoints, however, were based on interaction energy calculations for colloid-planar surface interactions. Recent studies (Shen et al., 2012a, 2019a; Bradford and Torkzaban, 2013; Zou et al., 2015; Torkzaban and Bradford, 2016) showed that colloids attached atop NPAs can also be detached from primary energy minima by IS reduction. This is because the NPAs can reverse the trend for the variation of the primary minimum depth with solution IS (Shen et al., 2019a). Specifically, the primary minimum depth can decrease with decreasing solution IS with the presence of NPAs. The primary minimum can even disappear from interaction energy profiles at low ISs due to the NPAs. In this case, the interaction energy decreases monotonically with separation distance and the colloid experiences repulsive forces at all separation distances (Wang et al., 2019). Therefore, the colloids initially attached atop NPAs at high ISs via primary minimum association will be detached at the low ISs.

It should be noted that nanoscale charge heterogeneity has also been frequently used to explain the detachment by IS reduction (Pazmino et al., 2014; Rasmuson et al., 2017). These studies indicate that detachment of colloids from nanoscale chemical heterogeneity could occur because the repulsion between a colloid and bulk surface may exceed the attraction between the colloid and chemical heterogeneity at low ISs. Shen et al. (2018), however, demonstrated that whether the surface charge heterogeneity is present on surfaces or not does not change the trend for the variation of primary minimum depth with the solution IS (i.e., the increase of primary minimum depth with decreasing IS). In fact, the nanoscale surface chemical heterogeneity increases the primary minimum depth at all solution ISs under unfavorable conditions, causing the attachment at primary minima even more irreversible. Therefore, the detachment of nC_{60} NPs by reduction of IS should be mainly due to NPAs. The absence of detachment for the nC_{60} NPs initally attached at 100 mM $CaCl_2$ indicates that the nC_{60} NPs could not be released even if they were initially attached atop NPAs. This is likely due to the reason that the high concentration of Ca^{2+} resulted in strong interactions of the nC_{60} NPs with the NPAs via cation bridge.

As shown in Fig. 2 and Table 3, more detachment of nC_{60} NPs occurred in phase 3 if they were initially attached in the presence of HA under all conditions except in 100 mM $CaCl_2$. The results clearly indicate that the HA not only inhibited attachment (i.e., increase of C/C_0 in phase 1 of BTCs), but also caused more weak attachments. The nC_{60} NPs via the weak adhesions were subsequently detached by IS reduction. Table 2 shows that the presence of HA reduced the depths of primary minima and accordingly adhesive forces and torques. The HA can even cause the decrease of primary minimum depth with decreasing solution IS for the colloid-planar surface interactions due to exerting steric repulsions (i.e., similar to the NPA effects) (Wang et al., 2016a, 2016b). The nC_{60} NPs would be detached with lowering IS if the adhesive torques were overcome by hydrodynamic torques (Wang et al., 2016a). The reduction of primary minimum depth and adhesive force/torque by HA could assist the detachment of colloids attached especially atop NPAs. Specifically, previous studies (Bradford et al., 2013; Shen et al., 2015, 2019a) showed that the variation of densities and curvatures of NPAs caused a distribution of primary minimum depth. The nC_{60} NPs that remained attached at low ISs atop some NPAs may be detached if the HA was present and the adhesive torques were

reduced to be smaller than hydrodynamic torques. The increased detachment by HA could also be due to the enhanced disaggregation of the aggregated nC_{60} NPs. This is because the presence of HA could cause decrease of primary minimum depth with IS reduction for the colloid-colloid interaction in the presence the steric repulsion (Omar et al., 2014; Shen et al., 2019a). The absence of nC_{60} NPs detachment at 100 mM $CaCl_2$ indicates that the presence of Ca^{2+} with high concentrations caused very stable complex of nC_{60} NPs and HA (see Fig. 4) and strong interactions between the complex and surfaces (Schijven and Hassanizadeh, 2002; Chen and Elimelech, 2007, 2008; Zhang et al., 2012; Chen et al., 2014).

4. Conclusions

Through carrying out column experiments under saturated conditions, we found that the HA reduced the attachment of nC_{60} NPs in sand (particularly on NPAs). However, the influence of HA on attachment was dependent on solution chemistry. Specifically, the reduction of attachment was significant only in 10 mM NaCl and 1 mM $CaCl_2$. There was no influence of HA on the attachment in 100 mM NaCl and 10 and 100 mM $CaCl_2$ (i.e., complete attachment both in the absence and presence of HA). The reduction of attachment was attributed to the decrease of attachment atop some NPAs where the primary minimum wells were shallow and the attachment was readily influenced by the HA. At 100 mM NaCl and 10 and 100 mM $CaCl_2$, the primary minima became deep atop the NPAs even in the presence of HA and thus no influence of HA on attachment was observed. The detachment was more upon reduction of solution IS if the nC_{60} NPs were initially attached in the present of HA under all chemical conditions expect at 100 mM $CaCl_2$. The results indicate that HA caused a fraction of nC_{60} NPs weakly attached on sand surfaces via primary-minimum association and then detached by reducing solution IS. However, very stable complex of HA and nC_{60} NPs existed and the interaction of the complex with the sand surfaces was strong at 100 mM $CaCl_2$, causing no detachment. The attachment was also irreversible on large charge heterogeneities or concave surfaces due to deep primary minimum wells at all ISs.

The aforementioned reversible attachment at primary minima by HA could cause the travel distance of NPs very long in subsurface environments by continuous capture and release (e.g., when multiple rainfall events occur). As such, the mobilization of the NPs will be underestimated in the presence of HA if the mathematic model (e.g., the convection-diffusion equation incorporating a term of first-order kinetic interaction with a reduced rate coefficient) only considers the inhibited attachment. In addition, when using membranes for water treatment, attached colloids on membrane surfaces in formal treatment may detach during the next treatment with the assistance of HA, causing the water contaminations. Therefore, our work has important implication to accurate prediction of fate and transport of NPs and NP-associated contaminants in subsurface environment and use of membranes for water and wastewater treatment.

Declarations of Competing Interest

None.

Acknowledgements

This work was supported by the National Natural Science Foundation of China (41671222, 41922047), and National Key Research and Development Program of China (2017YFD0800300).

References

Bai, C.M., Eskridge, K.M., Li, Y.S., 2013. Analysis of the fate and transport of nC_{60} nanoparticles in the subsurface using response surface methodology. J. Contam. Hydrol. 152, 60–69.
Bhattacharjee, S, Elimelech, M, 1997. Surface element integration: a novel technique for evaluation of DLVO interaction between a particle and a flat plate. J. Colloid Interface Sci. 193, 273–285.
Bradford, S.A., Torkzaban, S., 2013. Colloid interaction energies for physically and chemically heterogeneous porous media. Langmuir 29, 3668–3676.
Chae, S, Badireddy, A R, Budarz, J F, Lin, S H, Xiao, Y, Therezien, M, Wiesner, M R, 2010. Heterogeneities in fullerene nanoparticle aggregates affecting reactivity, bioactivity, and transport. ACS Nano 4, 5011–5018.
Chae, S., Xiao, Y., Lin, S., Noeiaghaei, T., Kim, J., Wiesner, M.R., 2012. Effects of humic acid and electrolytes on photocatalytic reactivity and transport of carbon nanoparticle aggregates in water. Water Res. 46, 4053–4062.
Chen, K.L., Elimelech, M., 2006. Aggregation and deposition kinetics of fullerene (C_{60}) nanoparticles. Langmuir 22, 10094–11001.
Chen, K L, Elimelech, M, 2007. Influence of humic acid on the aggregation kinetics of fullerene (C_{60}) nanoparticles in monovalent and divalent nanoparticles in monovalent and divalent electrolyte solutions. J. Colloid Interface Sci. 309, 126–134.
Chen, K.L., Elimelech, M., 2008. Interaction of fullerene (C_{60}) nanoparticles with humic acid and alginate coated silica surfaces: Measurements, mechanisms, and environmental implications. Environ. Sci. Technol. 42, 7607–7614.
Chen, L X, Sabatini, D A, Kibbey, T C G, 2012. Transport and retention of fullerene (nC(60)) nanoparticles in unsaturated porous media: effects of solution chemistry and solid phase coating. J. Contam. Hydrol. 138, 104–112.
Cheng, X, Kan, A T, Tomson, M B, 2005. Study of C_{60} transport in porous media and the effect of sorbed C_{60} on naphthalene transport. J. Mater. Res. 20, 3244–3254.
Chrysikopoulos, C V, Syngouna, V I, 2014. Effect of gravity on colloid transport through water-saturated columns packed with glass beads: modeling and experiments. Environ. Sci. Technol. 48, 6805–6813.
Dhawan, A, Taurozzi, J S, Pandey, A K, Shan, W, Miller, S M, Hashsham, S A, Tarabara, V V, 2006. Stable colloidal dispersions of C_{60} fullerenes in water: evidence for genotoxicity. Environ. Sci. Technol. 40, 7394–7401.
Duncan, L K, Jinschek, J R, Vikesland, P J, 2008. C_{60} colloid formation in aqueous systems: effects of preparation method on size, structure, and surface, charge. Environ. Sci. Technol. 42, 173–178.
Franchi, A, O'Melia, C R, 2003. Effects of natural organic matter and solution chemistry on the deposition and reentrainment of colloids in porous media. Environ. Sci. Technol. 37, 1122–1129.
Haftka, J.J.-H., Bauerlein, P.S., Emke, E., 2015. Colloidal stability of (functionalised) fullerenes in the presence of dissolved organic carbon and electrolytes. Environ. Sci. 2, 280–287.
Hahn, M W, O'Melia, C R, 2004. Deposition and reentrainment of Brownian particles in porous media under unfavorable chemical conditions: some concepts and applications. Environ. Sci. Technol. 38, 210–220.
Hahn, M W, Abadzic, D, O'Melia, C R, 2004. Aquasols: on the role of secondary minima. Environ. Sci. Technol. 38, 5915–5924.
Hamaker, H.C., 1937. The London-van der Waals attraction between spherical particles. Physica 4, 1058–1072.
Hedayati, M., Sharma, P., Katyal, D., Fagerlund, F., 2016. Transport and retention of carbon-based engineered and natural nanoparticles through saturated porous media. J. Nanopart. Res. 18, 57. https://doi.org/10.1007/s11051-016-3365-6.
Hoek, E.M.V., Agarwal, G.K., 2006. Extended DLVO interactions between spherical particles and rough surfaces. J. Colloid Interface Sci. 298, 50–58.
Hogg, R., Healy, T.W., Fuerstenau, D.W., 1966. Mutual coagulation of colloidal dispersions. Trans. Faraday Soc. 62, 1638–1651.
Hyung, H., Fortner, J.D., Hughes, J.B., Kim, J.H., 2007. Natural organic matter stabilizes carbon nanotubes in the aqueous phase. Environ. Sci. Technol. 41, 179–184.
Jung, B, O'Carroll, D, Sleep, B, 2014. The influence of humic acid and clay content on the transport of polymer-coated iron nanoparticles through sand. Sci. Total Environ. 496, 155–164.
Klaine, S J, Alvarez, P J J, Batley, G E, Fernandes, T F, Handy, R D, Lyon, D Y, Mahendra, S, McLaughlin, M J, Lead, J R, 2008. Nanomaterials in the environment: behavior, fate, bioavailability, and effects. Environ. Toxicol. Chem. 27, 1825–1851.
Kroto, H.W., Heath, J.R., Obrien, S.C., Curl, R.F., Smalley, R.E., 1985. C_{60}: Buckminsterfullerene. Nature 318, 162–163.
Kümmerer, K., Menz, J., Schubert, T., Thielemans, W., 2011. Biodegradability of organic nanoparticles in the aqueous environment. Chemosphere 82, 1387–1392.
Kuznar, Z.A., Elimelech, M., 2004. Adhesion kinetics of viable *Cryptosporidium parvum* oocysts to quartz surfaces. Environ. Sci. Technol. 38, 6839–6845.
Li, Y.H., Wang, S.G., Wei, J.Q., Zhang, X., Xu, C., Luan, Z., Wu, D., Wei, B., 2002. Lead adsorption on carbon nanotubes. Chem. Phys. Lett. 357, 263–266.
Li, X Q, Zhang, P F, Lin, C L, Johnson, W P, 2005. Role of hydrodynamic drag on microsphere deposition and re-entrainment in porous media under unfavorable conditions. Environ. Sci. Technol. 39, 4012–4020.
Li, Y., Wang, Y., Pennell, K.D., Abriola, L.M., 2008. Investigation of the transport and deposition of fullerene (C_{60}) nanoparticles in quartz sands under varying flow conditions. Environ. Sci. Technol. 42, 7174–7180.
Li, Y., Liang, H., Yin, H., Sun, J., Cai, H., Rao, Z., Ran, F., 2005. Determination of fullerenes (C_{60}/C_{70}) from the Permian-Triassic boundary in the Meishan section of South China. Acta. Geol. Sinca. 79, 11–15.
Li, T., Jin, Y., Huang, Y., Li, B., Shen, C., 2017. Observed dependence of colloid detachment on the concentration of initially attached colloids and collector surface heterogeneity in porous media. Environ. Sci. Technol. 51, 2811–2820.
Li, Y., Koopal, L.K., Xiong, J., Wang, M., Yang, C., Tan, W., 2018. Influence of humic acid on transport, deposition and activity of lysozyme in quartz sand. Environ. Pollut. 242, 298–306.
Lin, S, Wiesner, M R, 2012. Deposition of aggregated nanoparticles-a theoretical and

experimental study on the effect of aggregation state on the affinity between nanoparticles and a collector surface. Environ. Sci. Technol. 46, 13270–13277.
Lin, D., Tian, X., Wu, F., Xing, B., 2010. Fate and transport of engineered nanomaterials in the environment. J. Environ. Qual. 39, 1896–1908.
Lin, D., Story, S.D., Walker, S.L., Huang, Q., Liang, W., Cai, P., 2017. Role of pH and ionic strength in the aggregation of TiO_2 nanoparticles in the presence of extracellular polymeric substances from Bacillus subtilis. Environ. Pollut. 228, 35–42.
McNew, C.P., LeBoeuf, E.J., 2015. The role of attached phase soil and sediment organic matter physicochemical properties on fullerene (nC_{60}) attachment. Chemosphere 139, 609–616.
McNew, C.R., LeBoeuf, E.J., 2016. nC_{60} deposition kinetics: the complex contribution of humic acid, ion concentration, and valence. J. Colloid Interface Sci. 473, 132–140.
Ninham, B W, 1999. On progress in forces since the DLVO theory. Adv. Colloid Interf. Sci. 83, 1–17.
Oberdorster, E., 2004. Manufactured nanomaterials (fullerenes, C_{60}) induce oxidative stress in the brain of juvenile largemouth bass. Environ. Health Perspect. 112, 1058–1062.
Oliveira, R, 1997. Understanding adhesion: a means for preventing fouling. Exp. Thermal Fluid Sci. 14, 316–322.
Omar, F M, Aziz, H A, Stoll, S, 2014. Aggregation and disaggregation of ZnO nanoparticles: influence of pH and adsorption of Suwannee River humic acid. Sci. Total Environ. 468–469, 195–201.
Pazmino, E., Trauscht, J., Johnson, W.P., 2014. Release of colloids from primary minimum contact under unfavorable conditions by perturbations in ionic strength and flow rate. Environ. Sci. Technol. 48, 9227–9235.
Porubcan, A.A., Xu, S., 2011. Colloid straining within saturated heterogeneous porous media. Water Res. 45, 1796–1806.
Qu, X., Alvarez, P.J.J., Li, Q., 2012. Impact of sunlight and humic acid on the deposition kinetics of aqueous fullerene nanoparticles (nC_{60}). Environ. Sci. Technol. 46, 13455–13462.
Rasmuson, A, Pazmino, E, Assemi, S, Johnson, W P, 2017. Contribution of nano- to microscale roughness to heterogeneity: closing the gap between unfavorable and favorable colloid attachment conditions. Environ. Sci. Technol. 51, 2151–2160.
Ryam, J N, Elimelech, M, 1996. Colloid mobilization and transport in groundwater. Colloids Surf. A Physicochem. Eng. Asp. 107, 1–56.
Sanchís, J., Berrojalbiz, N., Caballero, G., Dachs, J., Farré, M., Barceló, D., 2012. Occurrence of aerosol-bound fullerenes in the mediterranean sea atmosphere. Environ. Sci. Technol. 46, 1335–1343.
Sanchís, J., Bosch-Orea, C., Farré, M., Barceló, D., 2015. Nanoparticle tracking analysis characterisation and parts-per-quadrillion determination of fullerenes in river samples from Barcelona catchment area. Anal. Bioanal. Chem. 407, 4261–4275.
Sanchís, J., Aminot, Y., Abad, E., Jha, A., Readman, J., Farr, M., 2018. Transformation of C_{60} fullerene aggregates suspended and weathered under realistic environmental conditions. Carbon 128, 54–62.
Schijven, J F, Hassanizadeh, S M, 2000. Removal of viruses by soil passage: overview of modeling, processes, and parameters. Crit. Rev. Environ. Sci. Technol. 30, 49–127.
Schijven, J.F., Hassanizadeh, S.M., 2002. Virus removal by soil passage at field scale and groundwater protection of sandy aquifers. Water Sci. Technol. 46, 123–129.
Seetha, N., Hassanizadeh, S.M., Kumar, M.S.M., Raoof, A., 2015. Correlation equations for average deposition rate coefficients of nanoparticles in a cylindrical pore. Water Resour. Res. 51, 8034–8059.
Shen, C, Lazouskaya, V, Zhang, H, Wang, F, Li, B, Jin, Y, Huang, Y, 2012. Theoretical and experimental investigation of detachment of colloids from rough collector surfaces. Colloids Surf. A Physicochem. Eng. Asp. 410, 98–110.
Shen, C, Wang, L-P, Li, B, Huang, Y, Jin, Y, 2012a. Role of surface roughness in chemical detachment of colloids deposited at primary energy minima. Vadose Zone J. 11, 59–75.
Shen, C., Wang, F., Li, B., Jin, Y., Wang, L.P., Huang, Y., 2012b. Application of DLVO energy map to evaluate interactions between spherical colloids and rough surfaces. Langmuir 28, 14681–14692.
Shen, C, Lazouskaya, V, Zhang, H, Li, B, Jin, Y, Huang, Y, 2013. Influence of surface chemical heterogeneity on attachment and detachment of microparticles. Colloids Surf. A Physicochem. Eng. Asp. 433, 14–29.
Shen, C., Zhang, M., Zhang, S., Wang, Z., Zhang, H., Li, B., Huang, Y., 2015. Influence of surface heterogeneities on reversibility of fullerene (nC_{60}) nanoparticle attachment in saturated porous media. J. Hazard. Mater. 290, 60–68.
Shen, C, Bradford, S A, Li, T, Li, B, Huang, Y, 2018. Can nanoscale surface charge heterogeneity really explain colloid detachment from primary minima upon reduction of solution ionic strength? J. Nanoparticle Res. 20. https://doi.org/10.1007/s11051-018-4265-8.
Shen, C., Jin, Y., Zhuang, J., Li, T., Xing, B., 2019a. Role and importance of surface heterogeneities in transport of particles in saturated porous media. Crit. Rev. Environ. Sci. Technol. https://doi.org/10.1080/10643389.2019.1629800.
Shen, C., Zhang, W., Zeng, S., Shen, C., Jin, C., Huang, Y., 2019b. Interactions between nanoparticles and fractal surfaces. Water Res. 151, 296–309.
Taghavy, A, Pennell, K D, Abriola, L M, 2015. Modeling coupled nanoparticle aggregation and transport in porous media: a Lagrangian approach. J. Contam. Hydrol. 172, 48–60.
Tong, M., Ding, J., Shen, Y., Zhu, P., 2010. Influence of biofilm on the transport of fullerene (C-60) nanoparticles in porous media. Water Res. 44, 1094–1103.
Torkzaban, S., Bradford, S.A., 2016. Critical role of surface roughness on colloid retention and release in porous media. Water Res. 88, 274–284.
Wang, Y, Li, Y, Pennell, K D, 2008. Influence of electrolyte species and concentration on the aggregation and transport of fullerene nanoparticles in quartz sands. Environ. Toxicol. Chem. 27, 1860–1867.
Wang, Y., Li, Y., Kim, H., Walker, S.L., Abrioda, L.M., Pennell, K.D., 2010. Transport and retention of fullerene nanoparticles in natural soils. J. Environ. Qual. 39, 1925–1933.
Wang, Y., Li, Y., Costanza, J., Abriola, L.M., Pennell, K.D., 2012. Enhanced mobility of fullerene (C_{60}) nanoparticles in the presence of stabilizing agents. Environ. Sci. Technol. 46, 11761–11769.
Wang, Z, Wang, D, Li, B, Wang, J, Li, T, Zhang, M, Huang, Y, Shen, C, 2016a. Detachment of fullerene nC_{60} nanoparticles in saturated porous media under flow/stop-flow conditions: column experiments and mechanistic explanations. Environ. Pollut. 213, 698–709.
Wang, Z, Jin, Y, Shen, C, Li, T, Huang, Y, Li, B, 2016b. Spontaneous detachment of colloids from primary energy minima by Brownian diffusion. PLoS One 11, e0147368. https://doi.org/10.1371/journal.pone.0147368.
Wang, H., Zhang, W., Zeng, S., Shen, C., Jin, C., Huang, Y., 2019. Interactions between nanoparticles and fractal surfaces. Water Res. 151, 296–309.
Xie, B., Xu, Z., Guo, W., Li, Q., 2008. Impact of natural organic matter on the physicochemical properties of aqueous C_{60} nanoparticles. Environ. Sci. Technol. 42, 2853–2859.
Yang, K., Zhu, L.Z., Xing, B.S., 2006. Adsorption of polycyclic aromatic hydrocarbons by carbon nanomaterials. Environ. Sci. Technol. 40, 1855–1861.
Yang, Y., Nakada, N., Nakajima, R., Yasojima, M., Wang, C., Tanaka, H., 2013. pH, ionic strength and dissolved organic matter alter aggregation of fullerene C_{60} nanoparticles suspensions in wastewater. J. Hazard. Mater. 244-245, 582–587.
Yang, Q., Li, X., Zhang, L., Wang, G., Chen, G., Lin, D., Xing, B., 2019. Dispersion and stability of multi-walled carbon nanotubes in water as affected by humic acids. J. Mol. Liq. 279, 361–369.
Zhang, Y., Chen, Y., Westerhoff, P., Crittenden, J., 2009. Impact of natural organic matter and divalent cations on the stability of aqueous nanoparticles. Water Res. 43 (17), 4249–4257.
Zhang, L., Hou, L., Wang, L., Kan, A.T., Chen, W., Tomson, M.B., 2012a. Transport of fullerene nanoparticles (nC_{60}) in saturated sand and sandy soil: controlling factors and modeling. Environ. Sci. Technol. 46, 7230–7238.
Zhang, W., Isaacson, C.W., Rattanaudompol, U., Powell, T.B., Bouchard, D., 2012b. Fullerene nanoparticles exhibit greater retention in freshwater sediment than in model porous media. Water Res. 46, 2992–3004.
Zhang, W., Rattanaudompol, U., Li, H., Bouchard, D., 2013. Effects of humic and fulvic acids on aggregation of aqu/nC_{60} nanoparticles. Water Res. 47, 1793–1802.
Zhang, L., Zhang, Y., Lin, X., Yang, K., Lin, D., 2014a. The role of humic acid in stabilizing fullerene (C_{60}) suspensions. J. Zhejiang Univ. Sci. A 15, 634–642.
Zhang, L., Zhao, Q., Wang, S., Mashayekhi, H., Li, X., Xing, B., 2014b. Influence of ions on the coagulation and removal of fullerene in aqueous phase. Sci. Total Environ. 466-467, 604–608.
Zhou, D., Wang, D., Cang, L., Hao, X., Chu, L., 2011. Transport and re-entrainment of soil colloids in saturated packed column: effects of pH and ionic strength. J. Soil Sed. 11, 491–503.
Zhuang, J, Qi, J, Jin, Y, 2005. Retention and transport of amphiphilic colloids under unsaturated flow conditions: effect of particle size and surface property. Environ. Sci. Technol. 39, 7853–7859.
Zou, Y., Jayasuriya, S., Manke, C.W., Mao, G., 2015. Influence of nanoscale surface roughness on colloidal force measurements. Langmuir 31, 10341–10350.